Paper ID APEN-MIT-2020_171
Applied Energy Symposium: MIT A+B
August 12-14, 2020 • Cambridge, USA

Autonomous Nano-capsules for Subsurface Remediation and Energy Harvesting Applications

Afnan Mashat
EXPEC Advanced Research Center
Saudi Aramco
Dhahran, Saudi Arabia
afnan.mashat@aramco.com

Nan Shi
EXPEC Advanced Research Center
Saudi Aramco
Dhahran, Saudi Arabia
nan.shi@aramco.com

Amr I. Abdel-Fattah*
EXPEC Advanced Research Center
Saudi Aramco
Dhahran, Saudi Arabia
amr.abdelfattah@aramco.com

Abstract— An H-channel microfluidic device system was built to simulate the dead-end structures in subsurface environments. The accessibility to these restriction regions where significant amount of oil and contaminants may be trapped is challenging. Hence, large amount of unnecessary chemicals might be required for remediation and enhanced oil recovery (EOR) applications, making the process expensive and environmentally unfavorable. In this work, we demonstrate the ability of salinity gradients that naturally exist in the subsurface environment to target-migrate nano-capsules in porous and fractured rock formations. Our results demonstrate the concept and provide evidence of the potential of utilizing existing chemical and thermal gradients to enable autonomous and sustainable migration of nano-capsules into constricted regions in the subsurface environment for more efficient and environmentally-friendly subsurface remediation and energy harvesting applications.

INTRODUCTION

Remediation of subsurface groundwater aquifers and enhanced oil recovery (EOR) applications often involve the delivery of chemicals (surfactant, polymers, alkaline, etc.) to specific regions in the subsurface reservoir to mobilize oil or contaminants. Large volumes of oil and contaminants are trapped in tight pore spaces and pore throats. Accessing these constricted regions is challenging and may require injecting unnecessarily large amounts of chemicals to achieve some noticeable results, and to compensate for the loss of chemicals due to adsorption into the rock formation, making the process expensive and environmentally unfavorable [1].

The opportunities of using nano-materials in subsurface contaminants remediation [2] and EOR applications [3] has been -recently- recognized. One of the main challenges with those applications is the transport of treatment effectively to the target zone. To overcome the transport challenge, the autonomous migration of particles when exposed to chemical gradients i.e. diffusiophoresis (DP) can be exploited. DP enables faster and directed transport of nanoparticles into dead-end pore structure compared with pure diffusion [4]. This autonomous migration will reduce the cost of pumping as the migration is generated by harvesting the chemical gradients.

In this paper, we demonstrate that salinity gradients that naturally exist in the subsurface environment can transport nano-capsules in porous and fractured rock formations. This autonomous migration of nano-capsules marks a significant milestone towards the development of "target-delivery" agents that autonomously migrate in constricted regions in the reservoir without the aid of advective flows, thus the energy, machinery, and infrastructure needed to pump the chemicals into the subsurface formations. By utilizing the existing chemical background (i.e. salinity) in subsurface environment, we are providing a transport mechanism with minimal materials, operational cost, and carbon footprint.

Direct microscopic visualization experiments were conducted using microfluidic devices to evaluate the migration of nano-particles and nano-capsules. A microfluidic device with "H" geometry and in-situ formed dead-end channels was used to simulate the dead-end pores in subsurface regions, and was used to test the migration of polystyrene nano-particles (dispersed in DI water) under high-salinity water gradients. The speed and cumulative distance of the migration were obtained by analyzing high-resolution image sequences with micro particle image velocimetry (μPIV).

Results showed clear migration of polystyrene nano-particles up the salt gradient into the dead-end channel, driven by the chemical gradients established by the diffusion of electrolytes. By contrast, movement of polystyrene nano-particles motion was very slow without such electrolyte gradients. These results demonstrate the potential of using salinity gradients in delivering particles to dead-end regions.

MATERIALS AND METHODS

A. Fabrication of microfluidic device

A microfluidic device with an H-geometry was fabricated to simulate the dead-end pores in subsurface environment. The device was prepared following the standard "microfluidic stickers" method [5]. The microfluidic device was fabricated using a photo-curable glue (Norland optical adhesive 81, NOA81) bounded with a glass slide. The two main channels are 10000-μm long and 500-μm wide, connected by a thinner horizontal channel that is 6000-μm long and 200-μm wide (Fig 1, a).

B. Formation of dead-end channel

The dead-end channel was formed by - permanently - blocking one of the horizontal channel ends. First, the device was filled with high-salinity water (or any solution required being inside the dead-end channel). High-salinity water was synthesized using NaCl, $CaCl_2.2H_2O$, $MgCl_2.6H_2O$, Na_2SO_4 and $NaHCO_3$ [6]. Second, UV light (intensity 30 mW/cm^2)

was exposed in the targeted area of the horizontal channel. Third, a photo-curable glue; NOA-81 was injected through one of the main channel, once it reached the UV light an in-situ polymerization was occurred within few seconds (Fig 1, b-c) forming the dead-end channel (Fig 1, d). Finally, polystyrene nano-particles in low-salinity; DI water (or any other solution) are injected creating the gradients (Fig 1, e). The particles motion inside the dead-end channel is observed under the microscope (Fig 1, f), and recorded images are analyzed using micro-particle image velocimetry (μPIV).

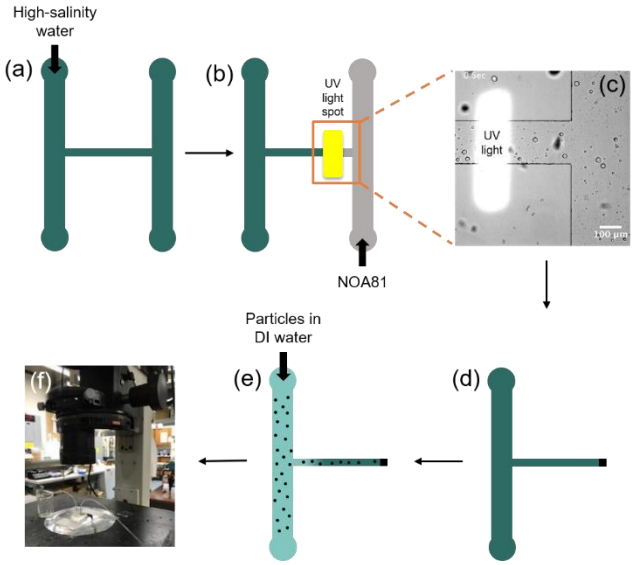

Fig 1. Fabrication of dead-end channel: (a) Schematic of the H-geometry microfluidic device structure consisting of two main channels that are connected horizontally by a thinner channel, filled with high-salinity water, (b) Injecting NOA-81 while UV light was spotted on the area to be blocked, (c) Close up micrograph of the right end of the horizontal channel where UV light was exposed. Once NOA-81 reached the UV, it will get polymerized yielding a dead-end channel blocked by the solid polymer, (d) The dead-end channel filled with high-salinity water, (e) Particles in DI water are injected creating the salinity gradients inside the dead-end channel, and (f) Image of the microfluidic device under the microscope to visualize the particles motion under the salinity gradients.

C. Validation of diffusive gradients in the dead-end channel

The concentration gradients in the dead-end channels established by the diffusion of a fluorescent dye (sodium fluorescein) was characterized. As the fluorescent dye (50 mg/250 mL) diffuses into a dead-end channel prefilled with DI water, the fluorescence intensity is recorded and analyzed with ImageJ to estimate the relative concentration of dye (Fig 2, a). We found that the fluorescence (concentration) profile is well described by the solution to 1D diffusion in semi-infinite space [6] (Fig 2, b).

$$\frac{\partial c}{\partial t} = D\frac{\partial^2 c}{\partial x^2} \tag{1a}$$

$$\hat{c}(x,t) = 1 - \mathrm{erf}(y) \tag{1b}$$

$$y = \frac{x}{\sqrt{4Dt}} \tag{1c}$$

where $\hat{c} = \frac{c - c_L}{c_H - c_L}$ is the scaled concentration by the concentration of diffusing solutions c_H and the initial concentration in the dead-end channel c_L. D is the diffusion coefficient and $x = 0$ corresponds to the entrance of dead-end channels.

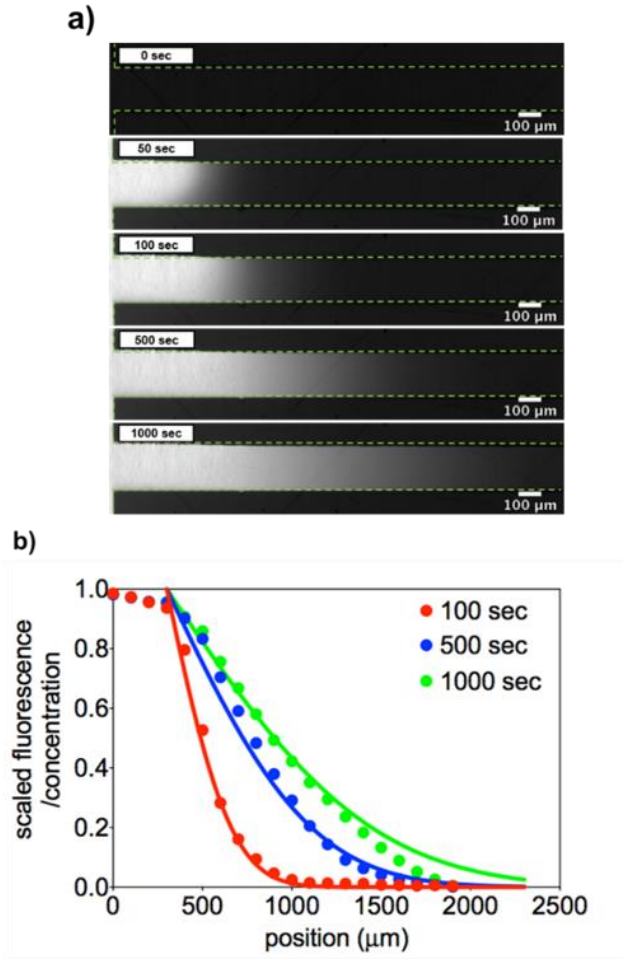

Fig 2. (a) Image sequences showing the fluorescent intensity distribution of sodium fluorescein inside the dead-end channel at different time points, (b) Temporal fluorescence profiles of fluorescein in the dead-end channel follow the diffusion equation given in Eq. (1).

RESULTS AND DISCUSSIONS

A. Establishing high-salinity gradients to deliver particles into dead-end channel

To simulate the dead-end pores in subsurface environment, the dead-end channel in the H-geometry microfluidic device was used to test the migration of particles under salinity gradients. The whole device was filled initially by high-salinity water followed by blocking the end of the horizontal channel forming the dead-end channel. Solution of polystyrene particles (dispersed in DI water) was injected through the main channel. Salinity gradient is created as the particles solution is injected and diffused into the channel causing the particles to move towards the high-salinity water inside the dead-end geometry. A sequence of images of the particles motion inside the dead-end channel at different time interval is shown in Fig 3. The diffusion of particles into the dead-end channel up the gradient can be clearly observed (Fig 3, b) compared to the control experiment where particles motion was very slow (Fig 3, a), (videos, supplementary information). Migration of particles is visualized (4X

objective) and recorded via Andor iXon Camera over a region that spans 2000 µm from the entrance of the dead-end channel.

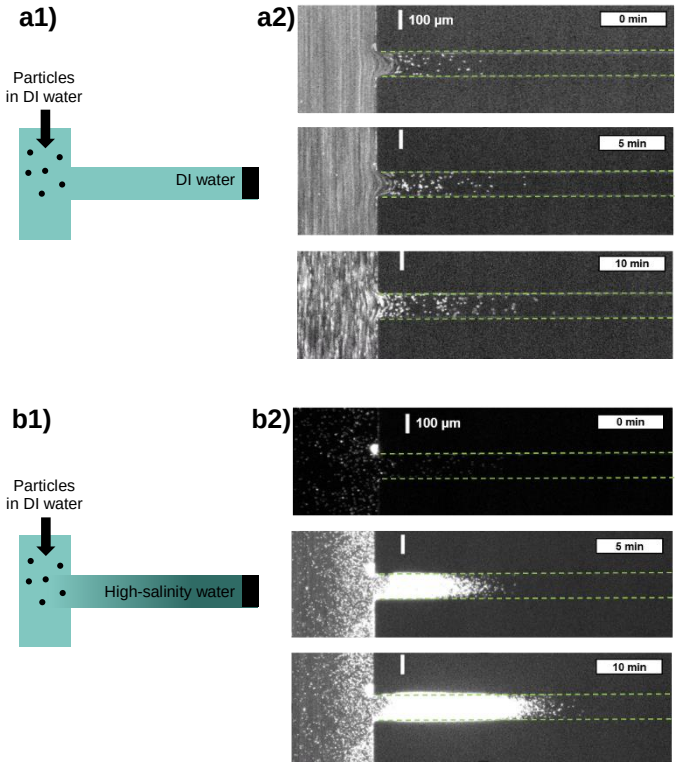

Fig 3. Schematic of (a1) dead-end channel of the control experiment where the dead-end channel was initially filled by DI water, (b1) dead-end channel initially filled by high-salinity water, (a2 & b2) Images sequences of the dead-end channel after injecting the particles. The particles motion is shown over time for the control and the actual experiments, respectively.

B. Quantitative analysis of the DP migration of particles

By introducing the chemical potential for each ion species i:

$$\mu_i = Z_i e\varphi + k_B T \ln n_B \tag{2}$$

we can write U_{DP} as the combined contribution of chemical potential and osmotic mobility from individual ion species:

$$U_{Dp} = \sum_i \nabla \mu_i^B M_i, \tag{3}$$

where Z_i is the valence of ions and φ is the electric potential.

Eq. (3) is a general expression of U_{DP} in terms of contribution from each ion species. The first term is the chemical potential gradient:

$$\nabla \mu_i = -Z_i e\, E_S + k_B T \nabla \ln n_i^B \tag{4}$$

that drives fluxes of ions in the bulk solution, where the spontaneous electric field E_S in multi-component solutions is given by:

$$E_S = \frac{\sum_i Z_i D_i \nabla n_i^B}{\sum_i Z_i^2 D_i n_i^B} \frac{k_B T}{e} \tag{5}$$

Importantly, E_S appears in the diffusion flux of each ion species,

$$J_i = -D_i \nabla n_i^B + \frac{Z_i D_i e}{k_B T} n_i^B E_S \tag{6}$$

so that mass transport of multiple diffusing ions is coupled. The second term in Eq. (3) is the osmotic mobility:

$$M_i = \frac{\epsilon}{\eta} \int_0^\infty z(n_i - n_i^B) dz \tag{7}$$

that depends on ion-particle interactions. n_i is the ions concentration in the electric double layer and z is the radial distance from the particle surface. Because $n_i = n_i^B$ as $z \to \infty$, M_i have finite values.

Finally, assuming equilibrium in the solution, $\mu_i = \mu_B$, leads to the Boltzmann distribution of n_i,

$$n_i(z) = n_i^B \exp\left(-\frac{\phi(z) Z_i e}{k_B T}\right) \tag{8}$$

in addition, the electrostatic potential φ in the solution follows the Poisson's equation,

$$\nabla^2 \phi(z) = -\frac{\rho_e}{\epsilon} = -\frac{e}{\epsilon} \sum_i Z_i n_i \tag{9}$$

gives the Poisson-Boltzmann equation,

$$\nabla^2 \phi(z) = -\frac{e}{\epsilon} \sum_i Z_i n_i^B \exp\left[-\frac{\phi(z) Z_i e}{k_B T}\right] \tag{10}$$

with boundary conditions $\phi = \zeta_p$ at $z = 0$ and $\partial\phi/\partial z = 0$ as $z \to \infty$. Solution to this equation yields profiles of $\phi(z)$ and $n_i(z)$, allowing the computation of M_i based on Eq. (7).

To predict particle migration in such gradients from Eq. (3), we first solve coupled diffusion of multiple ion species using MATLAB pde-solver PDEPE

$$\frac{\partial n_i^B}{\partial t} = \nabla \cdot \left(D_i \frac{\partial n_i^B}{\partial x} - \frac{Z_i e D_i}{k_B T} n_i^B E_S\right) \qquad i = 1,2,3,4,5 \tag{11}$$

where n_1^B, n_2^B, n_3^B, n_4^B, and n_5^B are denoted as the bulk concentration of Na+,Mg2+,Ca2+, Cl− and SO2− ions.

With Eq. (11), the general form of chemical potential gradients in Eq. (4) becomes

$$\nabla \mu_i^B = -Z_i e \tilde{\beta} \frac{k_B T}{e} + k_B T \nabla \ln n_i^B = k_B T(-Z_i \tilde{\beta} + \nabla \ln n_i^B) \tag{12}$$

in which $\tilde{\beta} = (\sum_i Z_i D_i \nabla n_i^B)/(\sum_i Z_i^2 D_i n_i^B)$. Substituting Eq. (12) into Eq. (3) gives

$$U_{DP} = \sum_i \nabla \mu_i^B M_i = \sum_i (-Z_i \tilde{\beta} + \nabla \ln n_i^B) k_B T M_i \tag{13}$$

Following the same procedure in the last section with $\lambda_D' = \sqrt{\epsilon k_B T / n_1^B e^2}$, we can write

$$k_B T\, M_i = \frac{k_B T}{\eta}\int_0^\infty z(n_i - n_i^B)dz$$

$$= \frac{k_B T}{\eta}\int_0^\infty n_i^B z\left[\exp\left(-\frac{Z_i\phi e}{k_B T}\right) - 1\right]dz$$

$$= \frac{k_B T}{\eta}\int_0^\infty n_i^B (\lambda_D')^2 \tilde{z}\left[\exp\left(-\frac{Z_\pm\phi e}{k_B T}\right) - 1\right]d\tilde{z} \quad (14)$$

$$= \left(\frac{k_B T}{\eta}\right)^2 \frac{\epsilon}{\eta}\frac{n_i^B}{n_1^B}\int_0^\infty \tilde{z}\left[\exp\left(-\frac{Z_i\phi e}{k_B T}\right) - 1\right]d\tilde{z}$$

Similarly, we non-dimensionalize the multi-ion Poisson-Boltzmann equation

$$\nabla^2\phi = -\frac{\rho_E}{\epsilon} = -\frac{\sum_i Z_i n_i^B e}{\epsilon} = -\frac{n_1^B e}{\epsilon}\sum_i \frac{n_i^B}{n_1^B} Z_i \exp\left(-\frac{Z_i\phi e}{k_B T}\right) \quad (15)$$

to the following form,

$$\tilde{\nabla}^2\tilde{\phi} = -\frac{n_1^B e^2 (\lambda_D')^2}{k_B T\,\epsilon}\sum_i \frac{n_i^B}{n_1^B} Z_i \exp\left(-Z_i\tilde{\phi}\right) = -\sum_i \frac{n_i^B}{n_1^B} Z_i \exp\left(-Z_i\tilde{\phi}\right) \quad (16)$$

The same boundary conditions, Eq. (15) - (16), are used to solve $\tilde{\phi}(\tilde{z})$, which is then substituted into Eq. (14) to compute M_i.

After expressing U_{DP} with n_i^B that depends on both time (t) and position (x), we can write particle migration in transient and multi-component gradients as

$$\frac{dx}{dt} = U_{DP}(x,t) \quad (17)$$

where x represents the migrating front of particles. Because direct integration of Eq. (17) is rather difficult in the current system, we simplify it with two assumptions: First, ζ_p remains constant in all ionic strength (similar to an effective zeta potential); Second, $U_{DP}(x,t)$ does not change significantly during a short time period, δt = 0.1 sec. Then we adopt forward Euler scheme to integrate Eq. (17), which yields a good prediction of particle migration dynamics assuming an effective $\zeta_p = -7.5$ mV (Fig 4).

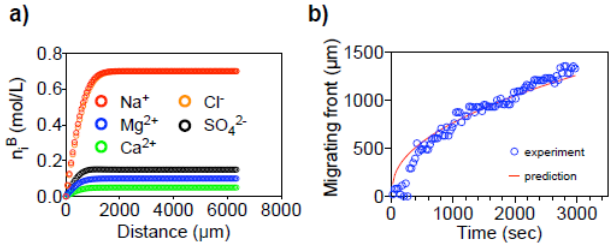

Fig 4. Predicted and measured particle migrating front. Measured migrating front (from the entrance of dead-end channel) is extracted by image analysis. Predicted migrating front is acquired by integrating Eq. (17).

CONCLUSION

Our results demonstrate the concept and provide evidence of the potential of utilizing existing chemical gradients to enable autonomous and sustainable migration of nano-capsules into constricted regions in the subsurface environment for more efficient and environmentally friendly subsurface remediation and energy harvesting applications. Those autonomous nano-capsules will overcome some of the current limitations associated with the delivery of chemicals to restricted regions:

- Chemical treatments are encapsulated inside the nano-capsules, target-delivered and released where they are most needed in subsurface formation thus, enabling the use of less chemicals while achieving the same results.
- The accessibility of nano-capsules to restricted regions where oil or contaminants are trapped will allow better recovery and higher removal efficiency.
- Nano-capsules travel autonomously to target regions in the formation via harvesting existing natural gradients allowing their deep penetration without pumping.
- The autonomous migration of nano-capsules is orders of magnitude faster compared to diffusion.

REFERENCES

[1] A. Muggeridge, A. Cockin, K. Webb, H. Frampton, I. Collins, T. Moulds and P. Salino, "Recovery Rates, Enhanced Oil Recovery and Technological Limits," *Phil. Trans. R. Soc. A*, 2014.

[2] T. Zhang, G. V. Lowry, N. L. Capiro, J. Chen, W. Chen, Y. Chen, D. D. Dionysiou and D. W. Elliott, "In Situ Remediation of Subsurface Contamination: Opportunities and Challenges for Nanotechnology and Advanced Materials," *Environ. Sci.: Nano*, vol. 6, no. 1283, 2019.

[3] M. Y. Rezk and N. K. Allam, "Impact of Nanotechnology on Enhanced Oil Recovery: A Mini-Review," *Ind. Eng. Chem. Res.*, vol. 85, pp. 16287-16295, 2019.

[4] A. Kar, T.-Y. Chiang, I. O. Rivera, A. Sen and D. Velegol, "Enhanced Transport Into and Out of Dead-End Pores," *ACS Nano*, vol. 9, no. 1, pp. 746-753, 2015.

[5] D. Bartolo, G. Degre, P. Nghe and V. Studer, "Microfluidic Sticker," *Lab Chip*, vol. 8, pp. 274-279, 2008.

[6] A. Mashat, A. I. Abdel-Fattah and A. Gizzatov, "NanoSurfactant: A Novel Nanoparticle-Based EOR Approch," *SPE Europec featured at 8th EAGE Conference & Exhibition* , 2018.

[7] R. B. Bird, W. E. Stewart and E. N. Lightfoot, Transport Phenomena, New York: John Wiley & Sons, 2001.